



## Mortar upscaling for multiphase flow in porous media

Małgorzata Peszyńska<sup>a</sup>, Mary F. Wheeler<sup>a</sup> and Ivan Yotov<sup>b</sup>

<sup>a</sup> *Texas Institute for Computational and Applied Mathematics, University of Texas, Austin, TX 78712, USA*  
E-mail: mpsz@ticam.utexas.edu

<sup>b</sup> *Department of Mathematics, University of Pittsburgh, Pittsburgh, PA 15260, USA*

Received 4 June 2001; accepted 14 December 2001

In mortar space upscaling methods, a reservoir is decomposed into a series of subdomains (blocks) in which independently constructed numerical grids and possibly different physical models and discretization techniques can be employed in each block. Physically meaningful matching conditions are imposed on block interfaces in a numerically stable and accurate way using mortar finite element spaces. Coarse mortar grids and fine subdomain grids provide two-scale approximations. In the resulting effective solution flow is computed in subdomains on the fine scale while fluxes are matched on the coarse scale. In addition the flexibility to vary adaptively the number of interface degrees of freedom leads to more accurate multiscale approximations. This methodology has been implemented in the Center for Subsurface Modeling's multiphysics multiblock simulator IPARS (Integrated Parallel Accurate reservoir Simulator). Computational experiments demonstrate that this approach is scalable in parallel and it can be applied to non-matching grids across the interface, multinumercs and multiphysics models, and mortar adaptivity. Moreover unlike most upscaling approaches the underlying systems can be treated fully implicitly.

**Keywords:** fully implicit, mixed finite element method, mortar spaces, multiblock, multiphase flow, multiphysics, porous media, upscaling

### 1. Introduction

A novel multiblock mortar methodology for modeling complex multiphysics phenomena occurring in energy and environmental applications allows for coupling different physical processes and different time discretizations in a single simulation [33]. This is achieved by decomposing the physical domain into a series of subdomains (blocks) and using independently constructed numerical grids and possibly different discretization techniques in each block. Physically meaningful matching conditions are imposed on block interfaces in a numerically stable and accurate way using mortar finite element spaces.

In this paper we establish a close connection between the mortar methodology and some recent upscaling procedures often referred to as *subgrid-scale* modeling [26,35,2] which treat linear steady-state or linearized transient problems. The motivation for these formulations is that fine scale features are often numerically unresolvable on practical finite element meshes. In [26], the original problem is decomposed into two

subproblems. First, fine scales are solved in terms of the coarse scale using numerical Greens functions. Second, a coarse scale problem is solved after incorporating the fine scale information into the coarse scale basis functions. A similar approach is taken in [35] for modeling heterogeneous structures and in [5,2] for modeling flow in porous media. The relation of subgrid modeling to stabilized finite element methods is discussed in [14].

The subgrid modeling can be viewed as an alternative to the classical upscaling problem for flow in porous media. In the latter the permeability field is given on a fine scale. Effective parameters are computed on a coarse scale and then used to carry out coarse scale flow simulations [20,15,13,1]. The connection between the subgrid modeling and the mortar approach can be established as follows. In the mortar framework the coarse grid is defined by the subdomain decomposition (i.e., each subdomain is an element of the coarse grid). The fine grid is the union of local subdomain grids. Note that this formulation allows for the fine grids to be non-matching from one coarse grid element to another. If the mortar space for matching fluxes across subdomains is chosen to consist of a single (bi)linear mortar function on each coarse edge (face), see figure 1, then the resulting solution may be thought of as an effective coarse grid solution which incorporates local (subdomain) fine grid information. We call this approach mortar upscaling. Unlike in traditional upscaling techniques, no effective parameters need to be computed. The computed solution is very similar to the one produced by the subgrid modeling method [2]. Our solution algorithm is based on solving a mortar interface problem (see section 2) and is therefore different from the algorithm employed in [2]. Some of the advantages of our approach are described below.

One advantage of the mortar interface formulation is that it provides the flexibility to adaptively vary the number of mortar degrees of freedom. As we show in our examples in section 5.1, finer mortar grids provide better accuracy [55,3], while coarser mortar grids lead to easier to solve algebraic problems [54,43,44]. The limiting case of using coarsest mortar space described above is the least expensive to solve. In highly heterogeneous large variation problems, however, it may be necessary to use finer mortar grids in parts of the domain for better flow resolution. A natural way of measuring the mortar upscaling error is to compute the flux jump in a finer mortar space. This can be used as an error estimator for adapting the mortar grids. The approach is closely related to some other techniques for hierarchical modeling of heterogeneous materials [58,25]. Our numerical tests in section 5.2 indicate that, with proper adaptivity, the increase in computational cost is only a fraction of the increase in the solution quality (measured by well rates, for example). The ability to measure the mortar upscaling error and to adaptively account for it provides an advantage to standard upscaling methods where the upscaling error is often difficult to estimate.

Some further advantages of the mortar formulation are demonstrated by the numerical experiments in sections 5.3 and 5.4. In particular, it is shown that substantial computational savings can be achieved without sacrificing accuracy by appropriately

choosing different physical models, (possibly non-matching) local grids, and different numerical methods on different subdomains.

The outline of the paper is as follows. In section 2 we briefly describe the single, two-phase, including both the sequential and fully implicit approach, and black-oil model formulations. In section 3 we formulate the multiblock multimodel technique, including subdomain and mortar interface algorithms for multiphase flow. In section 4 we describe the computational framework called IPARS (Integrated Parallel Accurate Reservoir Simulator), which has been employed in our mortar upscaling studies, and we show parallel scalability of the multiblock implementation. Computational studies which illustrate the flexibility of our mortar upscaling approach are discussed in section 5. Here we discuss mortar adaptivity, the coupling of explicit and implicit models, and the coupling of different physical models. In section 6 conclusions and extensions are presented.

## 2. Multiphase model formulation

In this section we briefly recall the conservation equations, constitutive laws and time discretization techniques. Our main focus is on the two-phase (water and oil) flow model in implicit and sequential form. Additionally, we consider an implicit three-phase (water, oil, and gas) black-oil model and an implicit single-phase (water) flow model which are used in multiphysics examples in section 5.4. Here the porosity  $\phi$  and permeability tensor  $K$  are spatially varying and constant in time reservoir rock data. Other rock properties involve relative permeability and capillary pressure relationships which are given functions of saturations and possibly also of position in the case of different *rock types*. The well injection and production rates are defined using the Peaceman well model [39] extended to multiphase and multicomponent flow, and they describe typical well conditions for pressure or rate specified wells.

Let the lower case subscripts w, o, and g denote the water, oil and gas phases, respectively, and the upper case subscripts W, O, and G the flowing components: water, heavy hydrocarbon or oil, and light hydrocarbon or gas, respectively. The corresponding phase saturations are denoted by  $S_w$ ,  $S_o$ , and  $S_g$ , the phase pressures by  $P_w$ ,  $P_o$ , and  $P_g$ , and component concentrations by  $N_w$ ,  $N_o$ , and  $N_g$ . The well injection/production rates of the components are denoted  $q_w$ ,  $q_o$ ,  $q_g$ .

Consider first the two-phase immiscible slightly compressible oil–water flow model in which concentrations and densities of oil and water phase are given by  $N_M = S_m \rho_m = S_m \rho_m^{ref} e^{c_m P_m}$  for each component,  $M = O, W$ , identified with a phase  $m = o, w$ , respectively. The discrete-in-time implicit mass conservation equation and Darcy’s law are

$$\frac{(\phi N_M)^{n+1} - (\phi N_M)^n}{\Delta t_{n+1}} - \nabla \cdot U_m^{n+1} = q_M^{n+1}, \quad (1)$$

$$U_m^{n+1} = \frac{K}{\mu_m} (\rho_m k_m)^{n+1} (\nabla P_m^{n+1} - \rho_m^{n+1} G \nabla D). \quad (2)$$

The single-phase model which describes the (saturated) flow of a (slightly compressible) fluid (water = aqua) may be considered as a special case of the two-phase system (1)–(2) with  $S_o = 0$ . On the other hand, the system (1)–(2) can be extended to the *black-oil* model [32,31]. See also [38,30,45,16,48,21,34,11]. In the black-oil model in addition to water and oil there is a gas component with  $N_G > 0$  which is dissolved in the oil phase. In addition at lower pressures there may exist a gas phase with  $S_g > 0$ . Here, the oil phase density depends on the pressure and on the amount of gas and we use the fluid-reservoir dependent formation volume factor  $B_m$  of phase  $m$  so that (if appropriate units are used) Darcy's law is now written as

$$U_m^{n+1} = \frac{K}{\mu_m} \left( \frac{k_m}{B_m} \right)^{n+1} (\nabla P_m^{n+1} - \rho_m^{n+1} G \nabla D). \quad (3)$$

Note that the *oil phase* flux  $U_o$  is composed of the *oil component* flux  $U_O$  and of the *gas component in oil phase* flux. The *total gas component* is composed of the gas component in the gas phase and of the gas amount dissolved in the oil phase. The latter is proportional to the oil concentration with proportionality constant  $R_o$  which is controlled from above by the pressure dependent solution gas–oil ratio at saturated conditions  $R_{so}$  given as reservoir data. The mass conservation equations for oil and gas components in the black-oil model are

$$\frac{(\phi N_O)^{n+1} - (\phi N_O)^n}{\Delta t_{n+1}} - \nabla \cdot U_O^{n+1} = q_O^{n+1}, \quad (4)$$

$$\frac{(\phi N_G)^{n+1} - (\phi N_G)^n}{\Delta t_{n+1}} - \nabla \cdot (U_g + R_o U_O)^{n+1} = q_G^{n+1}. \quad (5)$$

Additionally, the system satisfies a volume constraint; namely, that the sum of the saturations equals one. Additional constitutive relations involve the capillary pressure relations

$$P_{cow}(S_w) = P_o - P_w, \quad (6)$$

$$P_{cgo}(S_g) = P_g - P_o. \quad (7)$$

The space discretization of all these models is based on mixed finite element methods reduced to cell-centered finite differences (see section 3.2 for details). The time discretization for all the above models is implicit, namely backward Euler. The models use different primary unknowns: black-oil model uses  $P_w$ ,  $N_O$ ,  $N_G$  as primary unknowns, the two-phase model uses  $P_o$ ,  $N_O$  and the single-phase uses  $P_w$ . The nonlinear or quasilinear system of equations arising in some models are solved by the Newton method, and the Jacobian equation is solved by one of a suite of iterative solvers capable of handling nonsymmetric and nonpositive systems arising from the Jacobian, for example GMRES, with sophisticated two-stage preconditioners [18,22,29]. The Newton method stops when the residuals are less than a given tolerance  $\varepsilon$ .

The fully implicit formulation is unconditionally stable and permits the use of large time steps which may vary adaptively while keeping the error in mass conservation to minimum with a small  $\varepsilon$ . A major disadvantage of the fully implicit method is the

complexity of the Newtonian iteration, which may be costly. Other formulations known as *IMPES* (*implicit pressures, explicit saturations*) are attractive alternatives [7]. Related are methods of *total pressure* [38] or *streamlines–streamtubes* [8]. Most rely on the splitting of the model equations into the time lagged (formally) elliptic part and the parabolic–hyperbolic part. Some of difficulties which arise in these approaches involve treatment of compressibilities and of varying well patterns, and the stability and accuracy of the splitting.

In the IPARS two-phase sequential model we use the splitting which goes back to [19], where different time steps were proposed to be used for the pressure and for the concentration equations. The primary variables in this formulation are water pressure  $P_w$  and saturation  $S_w$ . The first equation defines the value of water pressure at the new time step  $P_w^{n+1}$  as a solution to the problem

$$-\nabla \cdot (K \lambda_t^n (\nabla P_w^{n+1})) = \nabla \cdot (K \lambda_o^n \nabla P_c(S_w^n)) - \nabla \cdot (K (\lambda_o^n \rho_o^n + \lambda_w^n \rho_w^n) G \nabla D) \quad (8)$$

where the oil, water, and total mobilities are  $\lambda_o = k_o/\mu_o$ ,  $\lambda_w = k_w/\mu_w$ , and  $\lambda_t = \lambda_o + \lambda_w$ . This equation arises after the mass conservation equations for two phases are added and discretized in time. For simplicity, we omit the well terms. Also, compressibility of the fluids is essentially ignored in the pressure equation and only accounted for in the saturation equation to follow. Using the values of  $P_w^{n+1}$ , the densities, the phase velocities or volumetric fluxes  $u_o$ ,  $u_w$  defined by  $U_m = \rho_m u_m$ , and the total velocity  $u_t = u_o + u_w$  are computed. Then the saturation equation

$$\begin{aligned} & \frac{\phi S_w^{n+1} \rho_w^{n+1}}{\Delta t_{n+1}^S} + \nabla \cdot \left[ K \frac{\lambda_o^n \lambda_w^n}{\lambda_t^n} P_c'(S_w^n) \nabla S_w^{n+1} \right] \\ & = \frac{\phi}{\Delta t_{n+1}^S} S_w^n - \nabla \cdot \left[ \frac{\lambda_w^n}{\lambda_t^n} u_t^n \right] - \nabla \cdot \left[ K \frac{\lambda_o^n \lambda_w^n}{\lambda_t^n} (\rho_w^n - \rho_o^n) G \nabla D \right] \end{aligned} \quad (9)$$

is solved for  $S_w^{n+1}$ . The time step  $\Delta t_{n+1}^S$  for the saturation may be much smaller than the pressure step or, alternatively, pressure solution can be skipped and redone only every  $K$  saturation steps, with  $K$  as large as 100. The saturation time step is limited by the CFL-type stability condition  $(v/\phi)(\Delta t/\Delta x) < 1$  on the time and spatial discretization steps  $\Delta t$ ,  $\Delta x$  in terms of the velocity  $v$  and porosity  $\phi$ .

The resulting set of two separate fully discrete equations (or more, if multiple saturation steps are used) is solved each by a simple iterative linear solver like Preconditioned Conjugate Gradient (PCG) for symmetric positive definite systems. Since the system (8)–(9) is effectively a linearized version of (1)–(2), the computational cost per time step is much lower, but again, the time step may be severely restricted for reasons of accuracy and stability.

### 3. Mortar interface couplings for multiphase flow

In this section we describe the coupling of the models from the previous section in a multiblock formulation. We assume that the simulation domain  $\Omega \subset \mathcal{R}^3$ , is decomposed

into a series of subdomains (*faultblocks, blocks*)  $\Omega_k, k = 1, \dots, n_b$ . Let  $\Gamma_{kl} = \partial\Omega_k \cap \partial\Omega_l$  be the interface between  $\Omega_k$  and  $\Omega_l$ . A physical model is associated with each block.

This domain decomposition formulation for mixed methods stems from the classical paper [24] and was extended to the non-matching grids with mortar spaces in [3].

### 3.1. Interface and boundary conditions

On each interface  $\Gamma_{kl}$  the following physically meaningful interface continuity conditions are imposed:

$$P_m|_{\Omega_k} = P_m|_{\Omega_l} \quad \text{on } \Gamma_{kl}, \quad (10)$$

$$[U_M \cdot \nu]_{kl} \equiv U_M|_{\Omega_k} \cdot \nu_k + U_M|_{\Omega_l} \cdot \nu_l = 0 \quad \text{on } \Gamma_{kl}, \quad (11)$$

where  $\nu_k$  denotes the outward unit normal vector on  $\partial\Omega_k$ . Equations (10) and (11) represent continuity of pressures and normal fluxes, respectively (the plus sign in (11) is due to the opposite orientation of the normals on the two subdomains and  $[\cdot]$  denotes the jump). The sets of phase indexes  $m$  and component indexes  $M$  for which the above conditions are imposed depend on the physical models imposed on the neighboring blocks. In particular, let  $\Gamma^1$  be the union of all interfaces for which at least one of the neighboring subdomain models is single-phase, let  $\Gamma^2$  be the union of all “two-phase/two-phase” and “two-phase/black-oil” interfaces, and let  $\Gamma^3$  be the union of all black-oil/black-oil interfaces. Equations (10) and (11) then hold for  $m = w$  and  $M = W$  on  $\Gamma^1$ , for  $m = w, o$  and  $M = W, O$  on  $\Gamma^2$ , and for  $m = w, o, g$  and  $M = W, O, G$  on  $\Gamma^3$ .

We assume for simplicity that the *no flow* condition  $U_M \cdot \nu = 0$  is imposed on  $\partial\Omega$ , although more general types of boundary conditions can also be treated, see [42].

Note that the above conditions lead to well posed systems only when all relevant phases are present. Otherwise, some other interface conditions involving variables other than pressures must be imposed. This occurs, for example, in the black-oil model in two-phase conditions: if the gas phase is absent but the gas component is present and it is dissolved in the oil phase (undersaturated conditions), then the interface conditions must involve gas concentration instead of gas pressure. This is because the gas pressure in such conditions is a simple translate of oil pressure at the residual gas saturation. A general and detailed discussion of such conditions is given in the forthcoming paper [33].

### 3.2. Multiblock discretization

The discretization in space is achieved through the use of the lowest order Raviart–Thomas mixed finite element spaces  $RT_0$  [46] on a rectangular partition  $\mathcal{T}_{h_k}$  of  $\Omega_k$ , where  $h_k$  is associated with the size of the elements. The  $RT_0$  spaces are defined on  $\mathcal{T}_{h_k}$  by

$$\begin{aligned} \tilde{V}_{h_k} &= \left\{ v = (v_1, v_2, v_3): v|_E = (m_1 x_1 + \beta_1, m_2 x_2 + \beta_2, m_3 x_3 + \beta_3)^T: \right. \\ &\quad \left. m_l, \beta_l \in \mathcal{R} \text{ for all } E \in \mathcal{T}_{h_k}, \right. \\ &\quad \left. \text{and each } v_l \text{ is continuous in the } l\text{th coordinate direction} \right\}, \\ V_{h_k} &= \left\{ v \in \tilde{V}_{h_k}: v \cdot \nu_k = 0 \text{ on } \partial\Omega_k \cap \partial\Omega \right\}, \\ W_{h_k} &= \left\{ w: w|_E = m: m \in \mathcal{R} \text{ for all } E \in \mathcal{T}_{h_k} \right\}. \end{aligned}$$

To impose the interface matching conditions (10)–(11) we introduce a Lagrange multiplier or mortar finite element space (see [12,9] for the standard finite element formulation). The *mortar spaces* technique is capable of handling non-matching grids across the interface. Mortar mixed finite element methods have been studied for elliptic problems in [55,3] and for the Stokes problem in [10]. Optimal convergence is also shown for the case of a degenerate parabolic equation arising in two-phase flow in porous media [56]. Multinumerics and multiphysics applications can be found in [43,44,32,41,33].

The mortar finite element space  $M_{h_{kl}}$  is defined on a rectangular grid  $\mathcal{T}_{h_{kl}}$  on  $\Gamma_{kl}$ , where  $h_{kl}$  is associated with the size of the elements in  $\mathcal{T}_{h_{kl}}$ . In this space we approximate the interface pressures and concentrations, and impose weakly the continuity of normal fluxes.

If the subdomain grids adjacent to  $\Gamma_{kl}$  match, we take  $\mathcal{T}_{h_{kl}}$  to be the trace of the subdomain grids and define the matching mortar space by

$$M_{h_{kl}}^m = \{ \mu: \mu|_e = m: m \in \mathcal{R}, \text{ for all } e \in \mathcal{T}_{h_{kl}} \}.$$

If the grids adjacent to  $\Gamma_{kl}$  are non-matching, the interface grid need not match either of them. A mild condition on  $\mathcal{T}_{h_{kl}}$  to guarantee solvability and accuracy of the numerical scheme must be imposed (see remark 3.3). We define our non-matching mortar space on an element  $e \in \mathcal{T}_{h_{kl}}$  by

$$M_h^n(e) = \{ m\xi_1\xi_2 + \beta\xi_1 + \gamma\xi_2 + \delta: m, \beta, \gamma, \delta \in \mathcal{R} \},$$

where  $\xi_l$  are the coordinate variables on  $e$ . Then, for each  $\Gamma_{kl}$ , we give two possibilities for the non-matching mortar space, a discontinuous and a continuous version, as

$$\begin{aligned} M_{h_{kl}}^{n,d} &= \{ \mu: \mu|_e \in M_h^n(e) \text{ for all } e \in \mathcal{T}_{h_{kl}} \}, \\ M_{h_{kl}}^{n,c} &= \{ \mu: \mu|_e \in M_h^n(e) \text{ for all } e \in \mathcal{T}_{h_{kl}}, \mu \text{ is continuous on } \Gamma_{kl} \}. \end{aligned}$$

We denote by  $M_{h_{kl}}$  any choice of  $M_{h_{kl}}^{n,d}$ ,  $M_{h_{kl}}^{n,c}$ , or  $M_{h_{kl}}^m$  (on matching interfaces).

### 3.3. A mortar mixed finite element method for the implicit two-phase model

Here we describe the multiblock mortar formulation of the implicit two-phase model as given by equations (1)–(2). The other models are discretized similarly. We omit the details.

We employ a variant of the mixed finite element method, the *expanded mixed method* following [6]. It has been developed for accurate and efficient treatment of irregular domains (see [6,4] for single block and [55] for multiblock domains). In the context of multiphase flow this method allows for proper treatment of the degeneracies in the diffusion term (see remark 3.1). See also [42].

For  $m = w, o$  we define

$$\tilde{U}_m = -\nabla P_m.$$

Then

$$U_m = -\frac{k_m K}{\mu_m} \rho_m (\tilde{U}_m + \rho_m G \nabla D).$$

The implicit in time equations on a subdomain  $\Omega_k$  at the time  $t_{n+1}$  are solved for  $U_{h,m}^{n+1}|_{\Omega_k} \in V_{h_k}$ ,  $\tilde{U}_{h,m}^{n+1}|_{\Omega_k} \in \tilde{V}_{h_k}$ ,  $P_{h,m}^{n+1}|_{\Omega_k} \in W_{h_k}$ ,  $N_{h,m}^{n+1}|_{\Omega_k} \in W_{h_k}$ , and  $P_{h,m}^{M,n+1}|_{\Gamma_{kl}} \in M_{h_{kl}}$  which satisfy, for  $1 \leq k < l \leq n_b$ ,  $M = O, W$ , and  $m = o, w$ ,

$$\int_{\Omega_k} \frac{(\phi N_{h,M})^{n+1} - (\phi N_{h,M})^n}{\Delta t^{n+1}} w \, dx - \int_{\Omega_k} \nabla \cdot U_{h,m}^{n+1} w \, dx = \int_{\Omega_k} q_m w \, dx, \quad w \in W_{h_k}, \quad (12)$$

$$\int_{\Omega_k} \tilde{U}_{h,m}^{n+1} \cdot v \, dx = \int_{\Omega_k} P_{h,m}^{n+1} \nabla \cdot v \, dx - \int_{\partial\Omega_k \setminus \partial\Omega} P_{h,m}^{M,n+1} v \cdot \nu_k \, d\sigma, \quad v \in V_{h_k}, \quad (13)$$

$$\int_{\Omega_k} U_{h,m}^{n+1} \cdot \tilde{v} \, dx = \int_{\Omega_k} -\frac{k_{h,m}^{n+1} K}{\mu_{h,m}} \rho_{h,m}^{n+1} (\tilde{U}_{h,m}^{n+1} + \rho_{h,m}^{n+1} G \nabla D) \cdot \tilde{v} \, dx, \quad \tilde{v} \in \tilde{V}_{h_k}, \quad (14)$$

$$\int_{\Gamma_{kl}} [U_{h,m}^{n+1} \cdot \nu]_{kl} \mu \, d\sigma = 0, \quad \mu \in M_{h_{kl}}. \quad (15)$$

*Remark 3.1.* Introducing the pressure gradients  $\tilde{U}_m$  in the expanded mixed method allows for proper handling of the degenerate (for  $S_m = 0$ ) relative permeability  $k_m(S_m)$  in (13)–(14) (the edge values are computed by upwinding). It also allows, even for a full permeability tensor  $K$ , for accurate approximation of the mixed method on each subdomain by cell-centered finite differences for  $P_o$  and  $N_o$ . This is achieved by approximating the vector integrals in (13) and (14) by a trapezoidal quadrature rule and eliminating  $\tilde{U}_{h,m}$  and  $U_{h,m}$  from the system [6,4].

*Remark 3.2.* The usual piecewise constant Lagrange multiplier space for  $RT_0$  leads to only  $O(1)$  approximation on the interfaces in the case of non-matching grids. With the above choice for mortar space, optimal convergence and, in some cases, superconvergence is recovered for both pressure and velocity (see [55,3] for single-phase flow and [56] for incompressible two-phase flow in global-pressure formulation).



*Remark 3.3.* A necessary condition for solvability of the scheme is that, for any  $\phi \in M_{h_{kl}}$ ,

$$Q_{h,k}\phi = Q_{h,l}\phi = 0 \Rightarrow \phi = 0, \quad (16)$$

where  $Q_{h,k}$  is the  $L^2$ -projection onto  $V_{h_k} \cdot \nu_k$ . This condition requires that the mortar grid is not too fine compared to the subdomain grids and is easily satisfied in practice (see [55,3] for details).

### 3.4. Reduction to an interface problem

For simplicity consider two blocks A and B with interface I. In the multiblock multimodel approach we can assign one model to the domain (block) A and possibly a different model to the block B. We seek the interface values of the *primary unknowns* or *primary variables* on I such that the fluxes of components match in a prescribed weak sense as in (15). The choice of the primary unknowns on the interface is problem dependent and it is motivated by the convergence properties, computational efficiency or coding convenience, see [41,43,32]. Note that any given set of interface primary unknowns can match or not match the set of subdomain primary variables in block A or block B.

For notational convenience in the discussion below, depending on the context, we will understand as “values” the values of primary unknowns (denoted by  $\Lambda$ ) or the values of their projections into suitable spaces. A similar convention applies to the values of the mass component fluxes denoted by  $Flux_M$  across I outward to subdomains, respectively, and to their jump across I denoted below as  $B(\Lambda)$ . Furthermore, the interface problem  $B(\Lambda) = 0$  is understood in a weak sense, as in (15). See [3,56] and references therein for details.

Consider now the case that both blocks A and B are assigned the two-phase model. Use  $(P_o, N_o)$  as the interface primary variables. Some restrictions apply, see [41,43,32]. The goal of the interface algorithm is to find, at every time step  $t_{n+1}$ , the interface values  $\Lambda = \Lambda^{n+1} = (P_o^{*,n+1}, N_o^{*,n+1})$  so that

$$B(\Lambda) = |Flux_o^A - Flux_o^B| + |Flux_w^A - Flux_w^B| = 0$$

or, practically,

$$B(\Lambda) < \xi, \quad (17)$$

where  $\xi$  is some prescribed (interface) tolerance and  $|\cdot|$  is a suitable norm.

The interface operator  $B(\Lambda)$  is a Dirichlet-to-Neumann map. Its evaluation requires the solution in parallel of subdomain problems with Dirichlet data  $\Lambda$  or solving (12)–(14), given the current guess  $\Lambda^{n+1} = (P_o^{*,n+1}, N_o^{*,n+1})$  with

$$\begin{aligned} P_o^{M,n+1}|_I &= P_o^{*,n+1}, \\ P_w^{M,n+1}|_I &= P_o^{*,n+1} - P_c(S_w^{*,n+1}), \end{aligned}$$

where the value  $S_w^{*,n+1}$  is found from the capillary pressure relationship (6). Once the subdomain problem is solved, the normal fluxes of oil and water  $Flux_o^A, Flux_w^A, Flux_o^B, Flux_w^B$  across I outward to A and to B, respectively, are computed and  $B(\mathbf{\Lambda})$  can be evaluated.

Note that each of the blocks can be assigned either the two-phase implicit model or the sequential model. In the latter case, one needs to find a map from the set of primary unknowns on the interface  $\mathbf{\Lambda}^{n+1} = (P_o^{*,n+1}, N_o^{*,n+1})$  to the set of primary unknowns in the subdomain for the sequential algorithm  $(P_w^{*,n+1}, S_w^{*,n+1})$ . This may be delicate, see [43].

Finally, the problem  $B(\mathbf{\Lambda}) = 0$  can be solved by various solvers appropriate for general nonlinear problems. In the results reported in this paper we use the inexact Newton–Krylov method for which the Jacobian  $B'(\mathbf{\Lambda})S$  is approximated by a finite difference and the equation to be solved in an interface Newton step is

$$B'(\mathbf{\Lambda})S \approx \frac{B(\mathbf{\Lambda} + \sigma S) - B(\mathbf{\Lambda})}{\sigma} = -B(\mathbf{\Lambda}), \quad (18)$$

see [51]. Several parameters determine the efficiency and convergence of this technique; see [23,27,28]. For lack of space we only comment on the optimal choice of  $\sigma$ . For the multiblock implicit scheme where all subdomain solvers are fully implicit the values of  $\sigma$  are controlled by the subdomain tolerance  $\varepsilon$ , and we used  $\sigma \approx 10^{-8}$  or less with  $\varepsilon \approx 10^{-10}$ . For the multiblock sequential scheme the optimal values, in the absence of  $\varepsilon$ , were rather large ( $\approx 10^{-4}$ ). Therefore it is hard to choose a “perfect”  $\sigma$  for multiblock coupling of implicit and sequential models. However, the fully implicit interface solution of the problem  $B(\mathbf{\Lambda}) = 0$  by inexact-Newton may not be optimal for such couplings; see remarks in section 5.3.

#### 4. Implementation

The physical models described above are built in IPARS framework [36,49,51, 52,50,53], which handles general input/output, memory management, grid generation, visualization, parallelism, etc. The code for interface algorithm has been merged with the framework. The framework can have multiple (fault) blocks (or subdomains), each of which may have associated its own physical model. The neighboring blocks are connected via an interface. The values of primary variables and fluxes are projected back and forth between subdomains and interface and the subdomain solvers with Dirichlet data are executed until the fluxes from the two sides match to a given tolerance. Unit conversion between different models may be necessary during projection. The near optimal scalability of IPARS black-oil model is demonstrated in [52].

For the subdomain cells adjacent to the interface, the Dirichlet boundary condition is applied using values of primary variables delivered by the interface code. Transmissibilities, mobilities, fluxes, etc. are computed and stored. The Dirichlet condition is applied to the Jacobian and residuals of the discrete system.

The linear solvers for different physical models can be either different or the same. A parallel GMRES solver has been extended for solving multiple models simultaneously. The basic idea for the extension is to expand the work space from a scalar to an array, so that each model has its own entry of work space.

The parallelism is the most delicate and interesting issue to tackle. The extension to multiblock is handled by MACE interface [37], and the code scales very well; see results below. For multimodel, in contrast to the traditional single model simulator, we need to use the MIMD (multiple instruction multiple data) paradigm. Here we use multiple MPI communicators [47,43,31].

*Parallel scalability of the multiblock implementation.* To test the parallel scalability, we consider waterflood in a relatively small reservoir  $324 \times 324 \times 16$  [ft] so that breakthrough occurs at about 350 days. The permeability field is layered with vertical permeability  $K_V = 20$  [md] everywhere except in the middle layer of  $K_V = 5$  [md]; ratio  $K_H/K_V = 10$ ; for other parameters see the appendix. The waterflood simulation with one injection and one production well proceeds up to 500 days with variable time steps up to 15 days. The grid used in this study is medium-coarse, and it is  $54 \times 54 \times 8$ , which gives the total of around 23 K cells which are evenly divided between 3 blocks = domains. The case is run on a parallel Linux PC cluster with a different number of processors between 1 and 9 and using either standard Ethernet network or a high speed Myrinet switch. This results in the computational time and the calculated parallel speedup as shown in figure 2. Speedup here is defined as the ratio of computational time on 1 processor to computational time on  $n$  processors with linear (ideal) speedup equal to  $n$ .

The results demonstrate that the multiblock code scales extremely well, and that it even achieves superlinear speedup in the case of Myrinet runs. This latter effect is due to the small communication costs and to the local caching of data which is not available in a single processor case because of the limited cache size. The decrease of efficiency with growing number of processors in the Ethernet case is a typical phenomenon which occurs because of fixed problem size and computation to communication costs (Amdahl's law). Of course, for cases larger than this one, the deterioration of speedup occurs for number of processors larger than here. We note that the notion of scaled speedup which is used in parallel testing of linear problems does not really apply to reservoir simulation, as the problem itself changes if the size and well placement change.

## 5. Numerical examples

In this section we discuss how various choices of (a) multiblock and model decompositions, (b) mortar grids, and (c) convergence criteria, affect the accuracy and efficiency of computations.

Clearly the efficiency of the multiblock procedure is dependent on the choice of interface preconditioners. In the case of single-phase flow, *balancing preconditioners* [17,40] have been shown to be “essentially optimal”; here the condition number depends on the  $\log(1 + H/h)$  where  $H$  is the subdomain size and  $h$  is mesh size. Thus for large problems domain decomposition scales linearly as the number of processors

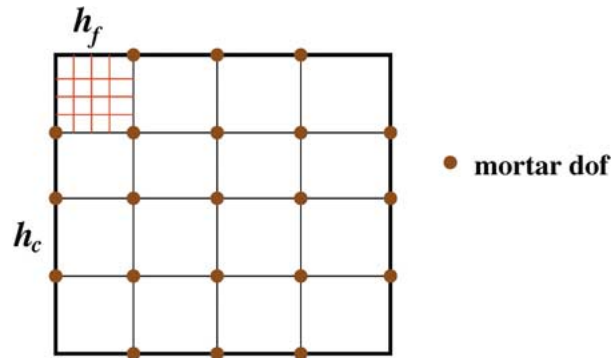


Figure 1. Two-scale discretizations.

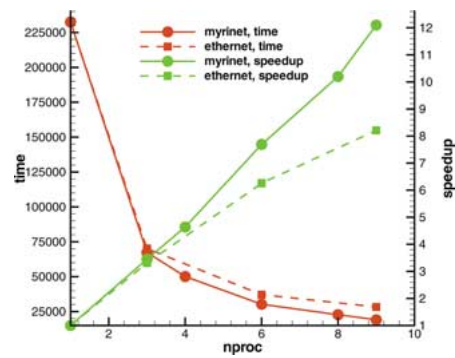
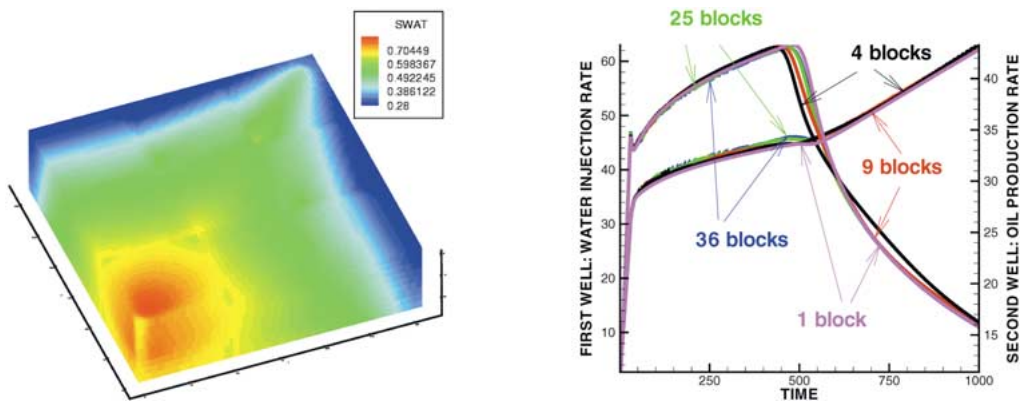


Figure 2. Parallel scaling of multiblock cases. Shown are total computational time [s] and speedup.

Figure 3. Fully implicit two-phase homogeneous case. Left: water saturation profiles after 961 days of waterflood for 9 blocks. Right: well rates. Used a fixed value of  $\xi = 0.1$ .

increases. Efficient preconditioners applicable to nonlinear problems associated with multiphase flow are a subject of current research [57] and are not yet available at this time. However, as we show below, the mortar multiblock technique offers flexibility in the use of different numerical and physical models and in addition it allows for mortar adaptivity. These features result in substantial savings in computational time.

### 5.1. Upscaling with varying number of blocks and of mortar degrees of freedom

Our basic example here is a three-dimensional quarter-five-spot problem on a  $315 \times 315 \times 27$  [ft] field with injection and production wells located close to lower left and upper right corners at around (16,16) (injector, 18 [ft] of open interval) and at (299,299) (producer, 27 [ft] open interval). Porosity is uniform and is equal to 0.2. Both oil and water are viscous and compressible, see appendix. The pressure gradient between the wells is initially at 30 [psi] and it increases to 260 [psi] at 30 days. First we study a simple homogeneous case whose purpose is to explain certain ideas about the mortar multiblock approach which are common to homogeneous and heterogeneous cases. The use of a homogeneous permeability field results in relatively smooth pressure and saturation fields which allow us to focus on the features of mortar multiblock approach rather than on the local behavior typical for heterogenous cases. The next example is heterogenous with coarse scale heterogeneity: here the permeability field resembles that of a fractured reservoir. In this example we show how, for two choices of the number of blocks, various choices of the number of mortar degrees of freedom and of convergence criteria affect the accuracy of computations and their efficiency.

#### 5.1.1. Homogeneous case

Here the permeability field is homogeneous with horizontal permeability equal to  $K_H = 100$  [md] and the vertical equal to  $K_V = 10$  [md]. With this, the breakthrough occurs at 500 days of waterflood, and the water/oil ratio reaches 3 at around 1000 days, see figure 3. The grid over the computational domain in this example is uniform, and it is  $90 \times 90 \times 9$  which totals 72900 cells. The domain is divided between 4, 9, 25 or 36 blocks, or we use the traditional 1 block setup. On each interface between any two blocks we use piecewise linear mortars on a  $1 \times 1$  mortar grid, see table 1. Note that, while

Table 1

Homogeneous case: well results and computation time over 1000 days normalized to 1 block solution.

| # blocks/# mortar<br>degrees of freedom | Computation<br>time (1000 days) | Values at 500 days |                   |                    | Breakthrough<br>time for water/oil<br>ratio = 0.1 |
|---|---------------------------------|--------------------|-------------------|--------------------|---|
|   |                                 | water inj.<br>rate | oil prod.<br>rate | water/oil<br>ratio |   |
| 1/-                                     | 1.0                             | 44.74              | 42.95             | 0.0056             | 543.692   |
| 4/16                                    | 1.54                            | 44.87              | 37.88             | 0.193              | 503.17  |
| 9/48                                    | 3.6                             | 44.76              | 40.01             | 0.132              | 520.308   |
| 25/160                                  | 2.046                           | 45.58              | 41.75             | 0.0835             | 532.15  |
| 36/240                                  | 1.44                            | 45.99              | 41.99             | 0.075              | 534.509   |

mass is conserved regardless of what mortar grid is used, the averaging procedure used in the projections between mortar grid and subdomain grid may lead to some local loss of accuracy. In addition, since Newtonian interface iteration is solved only up to a certain tolerance  $\xi$  as in (17), additional accuracy may be lost. In this example, we use  $\xi = 0.1$ .

Figure 3 shows saturation contours at time well after breakthrough obtained with the decomposition to 9 blocks as well as the well profiles for 1, 4, 9, 25, 36 blocks. Some of the well results are summarized in table 1, which additionally contains the associated computation time.

First, we discuss saturation contours. These exhibit local differences: note the higher water saturation values in the lower left corner of the production well block, which give an appearance of local heterogeneity but which are really a numerical artifact arising because of the averaging process onto the relatively coarse mortar grid. This phenomenon becomes less significant as the number of blocks grows and as, consequently, the mortar grid matches more closely the subdomain grid (for brevity, we do not show pictures for number of blocks other than 9).

There arises a question of the significance of this (local) loss of accuracy. Its impact on well rates is not profound, as can be seen in figure 3 and in table 1. In particular, engineers may be concerned not with the pointwise pressure or saturation values but rather with well rates which can be translated into economical value of recovery. These well rates clearly show the “convergence” of the case with a growing number of mortars to the single-block case which can be considered as a reference case. In addition, we see that this “convergence” comes at a cost, as the increased number of blocks/mortars requires more computation time.

In summary, the case with largest number of blocks appears to be most accurate and efficient even though, with today’s technology, it is not yet faster than a single-block solution. On the other hand, it offers a tremendous field for adaptivity, some of which will be discussed below.

### 5.1.2. Heterogeneous case

In this example we consider a heterogeneous permeability variant of the case above in which most of the waterflood follows the S-shaped “fracture” and the rest goes across the field, see figure 4. The permeability contrast is characterized by factor 40: all cells in blocks belonging to the “fracture” have horizontal permeability of 200 [md] and the others of 5 [md]. The ratio of horizontal to vertical permeability is  $K_H/K_V = 10$ . For other parameters, see appendix. Breakthrough in the heterogeneous case occurs later than in the homogeneous case, around 750 days.

Here we use a grid  $30 \times 30 \times 3$ , which is divided evenly either between (A) 4 or between (B) 25 blocks. While the decomposition in case B is aligned perfectly with discontinuities, the decomposition in case A is not and it can be regarded as the “worst scenario”. Furthermore, we use different mortar grids on the block interfaces, and we study the influence of the mortar discretization as well as of the convergence criteria on the quality of the solutions when compared to the traditional 1 block solution. Results are shown in table 2 and figure 6 which show well rates and computation time. In

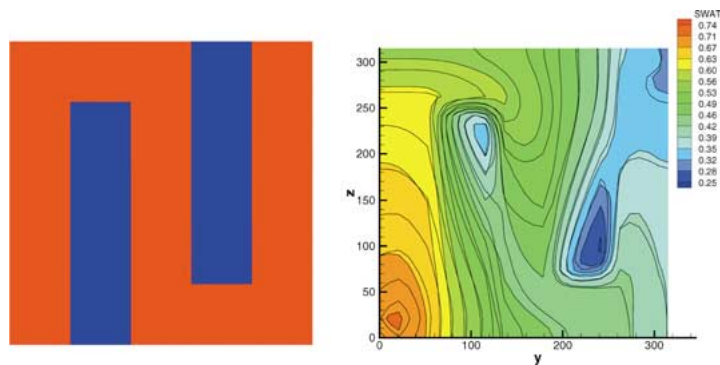


Figure 4. Heterogeneous case (fracture): permeability field (left) and water saturation contours after 1000 days of simulation for 1 block solution (right).

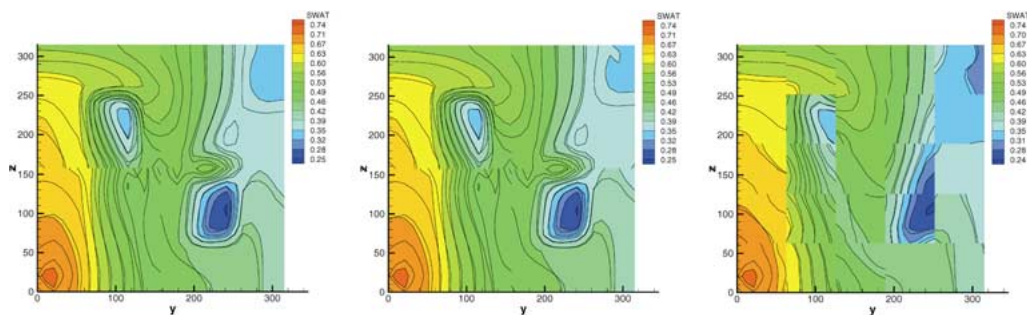


Figure 5. Heterogeneous case (fracture): water saturation contours after 1000 days of simulation. Case A (4 blocks,  $1 \times 3$  mortar grid) with  $\xi = 0.1$  (left), and  $\xi = 0.001$  (middle). Case B (25 blocks,  $1 \times 1$  mortar grid) and  $\xi = 0.1$  (right).

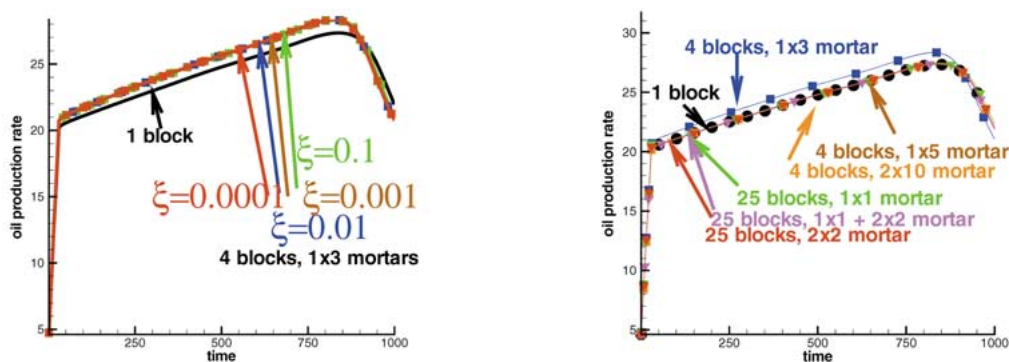


Figure 6. Heterogeneous case (fracture): comparison of well rates. Left: decomposition into 4 blocks with mortar grid  $1 \times 3$  and with varying  $\xi$ . Right: 4 and 25 block solutions for different mortar grids and with  $\xi = 0.1$  compared to 1 block solution.

Table 2  
Heterogeneous case (fracture): well results and computation time over 1000 days.

| # blocks/# mortar<br>degrees of freedom<br>(mortar grid) | Computation<br>time (1000 days) | Values at 500 days |                   |                    | Breakthrough                      |
|--|---------------------------------|--------------------|-------------------|--------------------|-----------------------------------|
|  |                                 | water inj.<br>rate | oil prod.<br>rate | water/oil<br>ratio | time for water/oil<br>ratio = 0.1 |
| 1/–  | –                               | 26.031             | 24.7759           | 0.050711           | 882.923                           |
| 4/32 (1×3) $\xi = 0.1$                                   | 1.0                             | 26.955             | 25.652            | 0.050715           | 873.399                           |
| 4/32 (1×3) $\xi = 0.01$                                  | 2.39                            | 26.953             | 25.653            | 0.050703           | 868.686                           |
| 4/32 (1×3) $\xi = 0.001$                                 | 2.59                            | 26.953             | 25.653            | 0.050703           | 868.972                           |
| 4/32 (1×3) $\xi = 0.0001$                                | 4.96                            | 26.953             | 25.654            | 0.050703           | 868.972                           |
| 4/48 (1×5) $\xi = 0.1$                                   | 1.18                            | 26.030             | 24.774            | 0.050722           | 887.2                             |
| 4/48 (1×5) $\xi = 0.01$                                  | 2.73                            | 26.031             | 24.775            | 0.050711           | 884.366                           |
| 4/132 (2×10) $\xi = 0.1$                                 | 1.91                            | 26.032             | 24.7759           | 0.050712           | 884.5                             |
| 4/132 (2×10) $\xi = 0.01$                                | 2.91                            | 26.032             | 24.777            | 0.050711           | 884.098                           |
| 25/160 (1×1)   | 1.18                            | 26.15              | 24.83             | 0.050903           | 888.315                           |
| 25/240 (1×1,2×2)   | 1.768                           | 26.107             | 24.81             | 0.050571           | 883.055                           |
| 25/360 (2×2)   | 1.67                            | 26.07              | 24.77             | 0.050594           | 885.582                           |

addition, contours of saturation projected onto the top plane are shown in figure 4 for the 1 block solution and in figure 5 for cases A and B. Note the discontinuity of profiles across block interfaces which arises from a combination of projection of 3D contours onto the 2D plane and from rendering of contours separately in each block. The former phenomenon is visible also for the 1 block case. The latter effect which only appears for multiblock can be overcome possibly with sophisticated post-processing tools which are not available to us at this time. It also becomes less significant for finer subdomain grids.

The choice of mortar grid  $1 \times 1$  corresponds here to 10 times more degrees of freedom in case B than in case A. This does not yield sufficient resolution in case A and may lead to 20% difference in well rates. Therefore the coarsest grid for A in this experiment is chosen to be  $1 \times 3$ . In addition, the location of mortar interfaces in these two cases is different: in particular it is more “natural” in case B, as the interfaces in this case are aligned with material discontinuities. For case B, we consider three different mortar grids: (i) coarse  $1 \times 1$  mortars, (ii) fine  $2 \times 2$  mortars and (iii) intermediate case in which the grid  $1 \times 1$  is used on “low velocity” interfaces and the grid  $2 \times 2$  is used on interfaces between high permeability blocks. It is then interesting to see how the results change with different numbers of degrees of freedom in each case. Moreover, we investigate the effect of varying the tolerance of the interface solver on the quality of the solutions.

Let us now briefly discuss the presented results. First, it is clear that in spite of significant differences in saturation profiles between case B and the 1 block solution as seen in figure 5, this decomposition into twenty five blocks offers high accuracy of well rates at relatively low cost, as seen in table 2. In addition, the coarsest mortar grid in this case provides enough resolution to achieve good agreement between well rates. On the



other hand, the mortar grid for case A must be chosen very carefully, since the quality of the results is critically dependent upon it, as shown by well rates. In addition, the convergence tolerance must be chosen appropriately: the saturation contours shown in figure 5 for case A with a small  $\xi$ , resemble 1 block solution better than those for case A with large  $\xi$ . Correspondingly, the material balances (not shown) for these two cases are correct to three significant digits for  $\xi = 0.1$  and to seven digits for  $\xi = 0.0001$ . However, the obtained well results do not differ significantly, but the computation cost is dramatically different. For case A, if about 4% discrepancy in well rates is acceptable, then it's advisable to use  $1 \times 3$  mortar grid. Otherwise, one should use  $1 \times 5$  mortar grid and  $\xi = 0.1$ .

In summary, this case shows that one can upscale the single-block solution by choosing a proper block decomposition which at best should be aligned with heterogeneities, and by using a relatively coarse mortar grid as well as liberal convergence criteria. In general, one can come up with an optimal decomposition and with optimal values of other parameters; however, such a selection is beyond the scope of this paper. An adaptive selection of mortars is discussed in the next section.

## 5.2. Mortar adaptivity for a highly heterogeneous case

In this example we study the accuracy and efficiency of the mortar upscaling technique applied to modeling flow in a highly heterogeneous reservoir. The permeability field is based on a model from the SPE Comparative Solution Upscaling Project (<http://www.pet.hw.ac.uk/research/csp/data-sets/set02.htm>). Oil–water displacement is simulated in a horizontal cross-section with dimensions  $1200 \times 2200$  [ft] at the bottom of the fluvial (Upper Ness) part of the reservoir. The fine grid ( $60 \times 220$ ) permeability (given in figure 7) has a mean value of 554 [md] and varies between 0.002 and 20000. An injection well is placed at (610, 425) and a production well is located at (630, 1825). We consider a 25 block decomposition ( $5 \times 5$ ) with each block discretized on the fine level. The results from three different runs are presented: a fine grid (1 block) simulation, a multiblock run with a single linear mortar element on each interface (coarse mortar), and a multiblock run in which the interfaces near the wells have been refined to 6 continuous linear mortar elements (adapted mortar). As can be seen from the oil pressure profiles (figure 8) and the oil concentration profiles (figure 9) after 2951 days of simulation, both mortar solutions approximate reasonably well the fine grid solution, with the adapted mortar capturing somewhat better some of the fine scale features of the flow. The adapted mortar solution reduces the production well rates discrepancy from the fine grid solution by factor of 2 compared to the coarse mortar, at the cost of increasing CPU time by 50%. These results indicate that higher accuracy can be achieved by appropriately adapting the mortar degrees of freedom, increasing only fractionally the computation cost. This flexibility of the mortar technique is especially useful in highly heterogeneous cases with large variations in the velocities. The implementation of a fully automated adaptive mortar procedure in IPARS is a subject of current research.

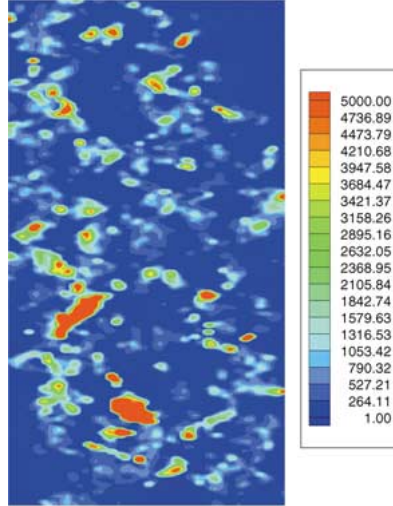


Figure 7. Permeability field for the highly heterogeneous example.

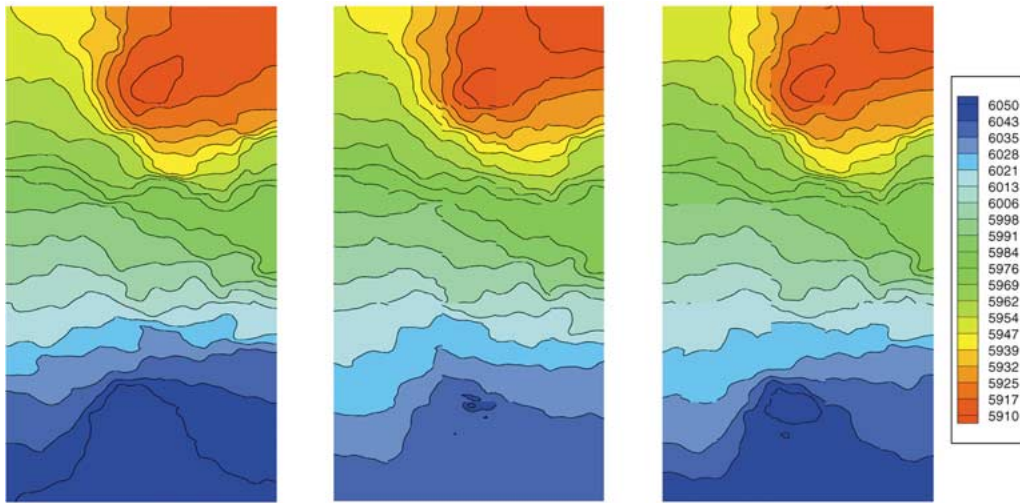


Figure 8. Oil pressure profiles after 2951 days: fine grid (left), coarse mortar (middle) and adapted mortar (right).

### 5.3. *Multinumerics example: coupling of explicit and implicit models for two-phase flow*

In this section we discuss the use of different numerical algorithms for two-phase flow in different subdomains (multinumerics) and we study the option of assigning the sequential model to some of the blocks. In all figures and tables in this section the sequential model is assigned the letter E and the implicit model is assigned the letter I. The major problem here is the design of an optimal interface solver. While an implicit

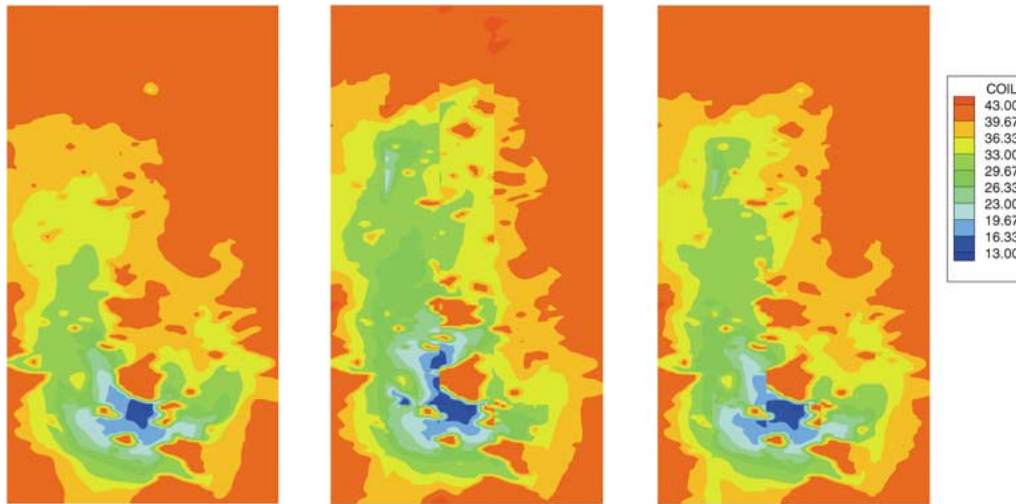


Figure 9. Oil concentration profiles after 2951 days: fine grid (left), coarse mortar (middle) and adapted mortar (right).

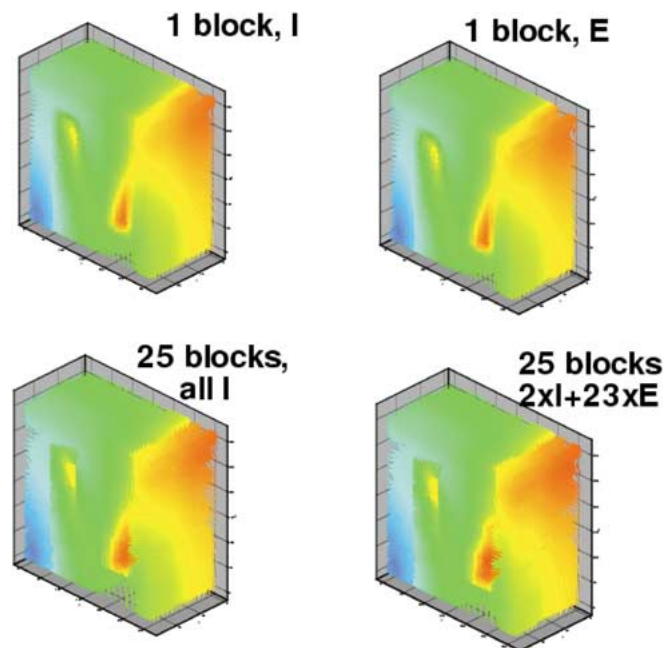


Figure 10. Multinumerics example: oil concentration profiles after 1000 days of simulation with 25 blocks and with different model decompositions (heterogenous case: fracture).

Table 3  
Timings for implicit model (I) coupled with sequential (E).

| Models in blocks           | Time [s]/iteration |               | Normalized # iterations |               |
|----------------------------|--------------------|---------------|-------------------------|---------------|
|                            | homogeneous        | heterogeneous | homogeneous             | heterogeneous |
| 25 I                       | 0.858              | 0.73          | 1.0                     | 0.92          |
| I (2, wells) + E (23)      | 0.177              | 0.242         | 2.01                    | 5.45          |
| I (1, prod. well) + E (24) | 0.193              | 0.221         | 0.94                    | 5.63          |

interface solver merges very well with implicit subdomain solvers, it appears that, by analogy, an IMPES-like approach and an appropriate preconditioner would be best to use on the interface for all blocks assigned to sequential model. On the other hand, it remains to be determined what structure of solver and preconditioner on the interface would be optimal when different models are used in different blocks. These are current research topics, and in this paper we restrict ourselves to the use of an implicit interface solver. In addition, for a multimodel parallel run, the optimal load balancing is determined on a case by case basis, see [31,32] which we did not attempt for the cases discussed in this paper.

The underlying example is a quarter-five-spot case from section 5.1. The grid is divided between 25 blocks and we assign the sequential model to some of the blocks and the implicit model is assigned to the remaining blocks. The well rates for homogeneous and for heterogeneous cAses are shown in figure 11 and table 3 contains the values of computational time per interface iteration. Here we only discuss most promising cases:

- (i) with implicit model assigned everywhere (25 I) or
- (ii) implicit model assigned around both wells (I, 2 wells), or
- (iii) implicit model assigned around the production well only (I, 1 well).

Well rates are also shown for the implicit model run without multiblock decomposition (I, 1 block) which is used as a reference case. In addition, we show oil concentration contours in figure 10 for some model decompositions.

In general we found that for a typical waterflood experiment, regardless of decomposition or models involved, the number of iterations on interface grows when front crosses the interface and that it is also large at first time steps, before pressure solution is established. The first phenomenon is obviously related to the variation in properties (mobilities and capillary pressure) across the front. Another observation is that because sequential model appears to give sharper fronts than the implicit, it is more advantageous to apply implicit model only “downstream” from the waterflood front. That is why, for the homogeneous case, the number of iterations for case (iii) is by a factor of 2 smaller than the count for case (ii). Note however that this phenomenon does not carry over to the heterogeneous case in which it is hard to predict the “path” of the front. As concerns the time per iteration, the results show that the smallest such quantity is obtained for the heterogeneous case in case (iii) as the number of cells assigned to the implicit model

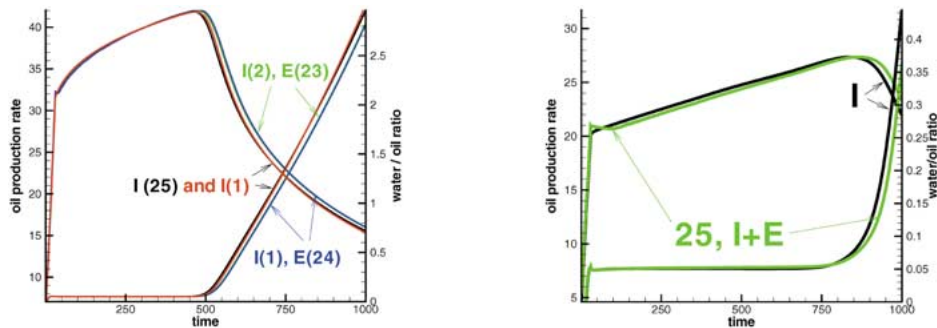


Figure 11. Multinumerics case: well rates for the homogeneous case (left) and for the heterogeneous case (right).

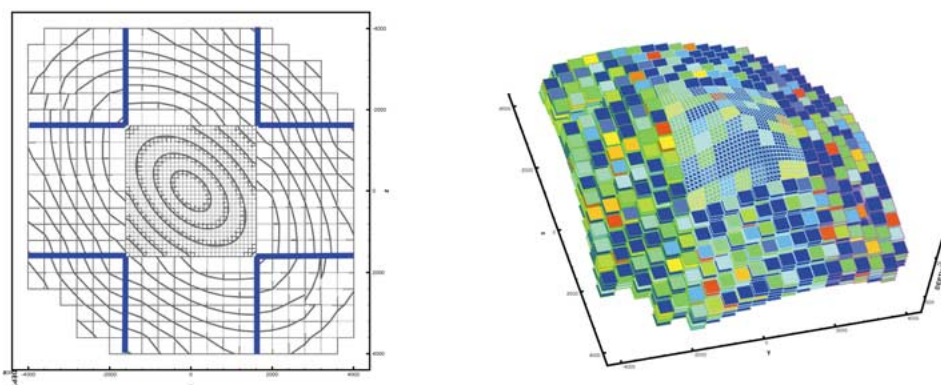


Figure 12. Field case: depth profiles, multiblock decomposition (left) and permeability field (right). Note fine grid in the center.

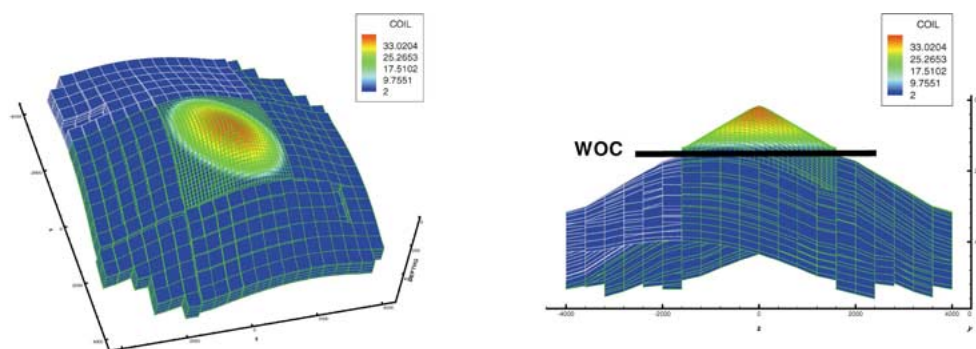


Figure 13. Field case: initial oil concentration profiles, two-phase case. Left: field view, right: side view.

appeared to be a decisive factor in the overall timings. At the same time, for the homogeneous case, the fastest setup per iteration was with implicit models around both wells.

However, the best accuracy or the closest match of the well rates with the ones obtained with no domain decomposition (1 block) was obtained when all blocks were assigned implicit model.

#### 5.4. Multiphysics example

In this section we demonstrate the flexibility of multiblock mortar implementation for local grid refinement with nonmatching grids and with the use of multiphysics.

The example is synthetic with geometry of the case constructed from data on Khursaniyah field [34], see figure 12. The reservoir occupies a portion of a parallelepiped of size  $8000 \times 8000 \times 700$  [ft] and it is dipping non-uniformly in all directions from its center and it is surrounded by impermeable strata; the permeability field is heterogeneous and uncorrelated, with mean  $K_V = 10$  [md] with ratio of horizontal to vertical equal  $K_H/K_V = 10$ . In the center part we use fine grid to capture depth variations in phase saturations. The use of coarse grid in the center block leads to overly simplified flow results and will result in up to 10% discrepancies in the well rates with respect to the fine grid case. With the described depth variations, the water–oil contact (WOC) occurs around depth 160 [ft], see figure 13, and so a large part of the reservoir is essentially an aquifer. The center part of the reservoir is where recovery takes place with 4 production wells and 2 injection wells that maintain pressure. Location of wells on pictures can be seen in figure 16.

Without multiblock decomposition, the use of fine grid in the center mandates the use of fine grid essentially everywhere. With multiblock decomposition we use 9 blocks. Center block has fine grid and all remaining 8 blocks have coarse grid and grids do not match across the interface.

We set up two different physical examples:

(A) *Two-phase.* In this example, the cells in the center block are in two-phase conditions  $0 \leq S_w \leq 1$  and the cells in the surrounding blocks are in single phase conditions. As a result of waterflood, the oil is swept of the middle part of the reservoir towards wells, see figure 14. Note appearance of pockets of oil. The distribution of fluids requires the use of at least of a two-phase code and we use the two-phase implicit model here.

(B) *Three-phase.* This example is similar except that we assume that the oil in the center blocks is saturated with gas and that in addition, at the top of the reservoir there is a small gas cap with  $S_g > 0$ . Initially, the gas cap is at  $S_g = 0.61$  and during the simulation, it decreases to  $S_g = 0.11$ , see figure 16. Note lower oil concentration in region where the gas cap resides. The presence of gas here requires the use of a black-oil model.

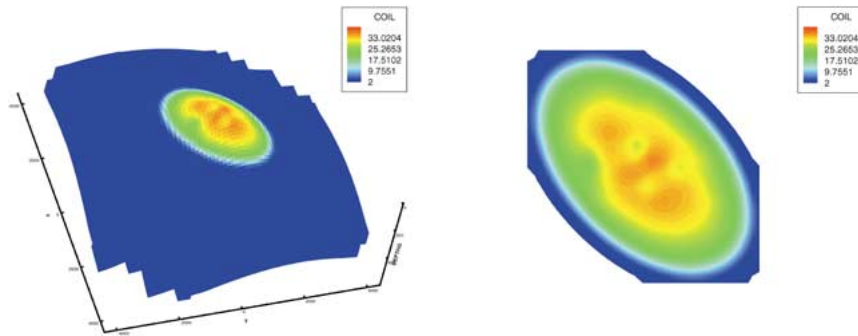


Figure 14. Field case: oil concentration profiles after 1000 days for two-phase case. Left: field view, right: zoomed aerial view.

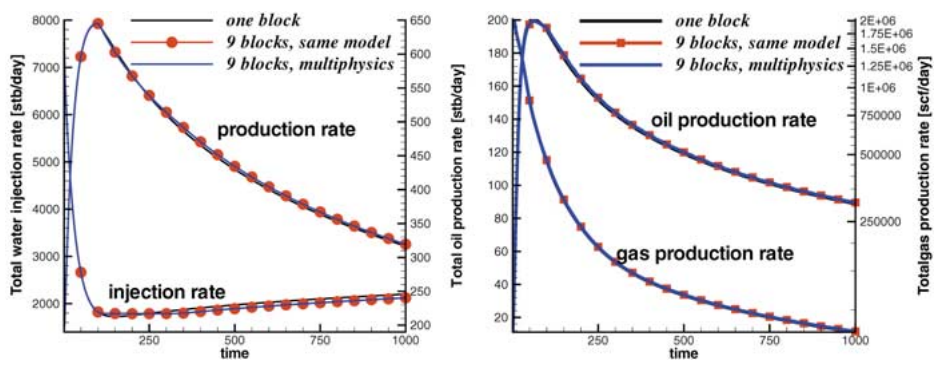


Figure 15. Field case: selected well rates for two-phase example (left) and three-phase example (right) for cases used in timing studies as in table 4.

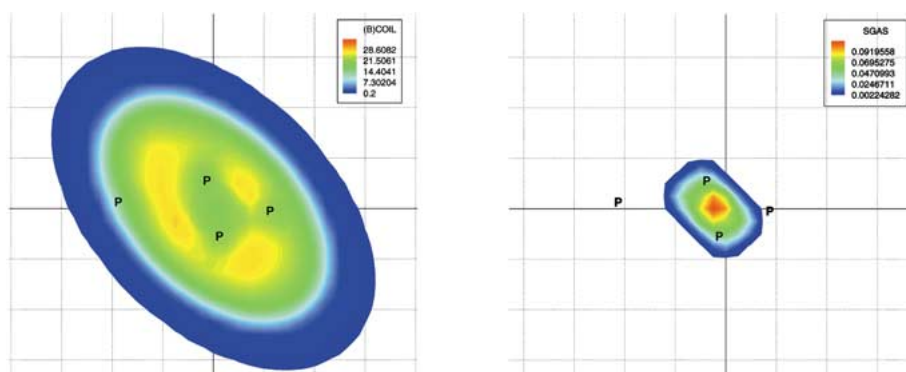


Figure 16. Field case: oil concentration (left) and gas saturation (right) profiles after 1000 days in zoomed aerial view (right) for three-phase case.

Table 4  
Timings for the field case [s].

| Models in blocks                              | Time/1000 days |                  |
|---|----------------|------------------|
|   | two-phase case | three-phase case |
| Fine grid everywhere, 1 block                 | 17766.855      | 52728.422        |
| Refined(center) + coarse(off-center)          | 5863.910       | 5781.920         |
| Same model in all blocks                      |                |                  |
| Refined(center) + coarse(off-center)          | 4623.780       | 4715.930         |
| Multiphase in center, single-phase off-center |                |                  |

Both of these cases can be run using different simulation scenarios, possibly adjusting the model and discretization to the objectives and resources available. We discuss the following scenarios:

- (i) fine grid everywhere and one block, one model and
- (ii) fine grid in the center block and coarse grid in the others, multiblock mortar solution with one model, and
- (iii) like (ii) but with single-phase model in all blocks but the center block.

Table 4 contains the timings for the simulation setup (i), (ii), and (iii). For simplicity, we used uniform permeability field and rectangular domains. Also, the same subdomain nonlinear and linear solver criteria and preconditioner parameters were used, with fixed  $\xi = 0.1$ . The most efficient block and model decomposition appears to be (iii), as expected.

## 6. Conclusions

We present a multiblock formulation for multiphase flow in porous media which provides a framework for coupling different physical models, different numerical methods, and non-matching grids in a single simulation. This flexibility allows for a substantial reduction of the computational cost of complex simulations (by appropriately choosing physical models and discretization schemes in different parts of the domain) without sacrificing accuracy. In the case of a single mortar element on each interface, our scheme computes an effective flow field based on fine scale subdomain solutions and coarse scale flux matching. Adaptivity in the mortar spaces provides a more accurate solution at only fractionally increased cost.

## Acknowledgements

We would like to thank several colleagues from the Center for Subsurface Modeling for their work on multiblock IPARS, in particular, we would like to acknowledge Manish Parashar, Qin Lu and John Wheeler. We also thank anonymous reviewers for their comments which helped us to improve the presentation in the paper.



Małgorzata Peszyńska and Mary F. Wheeler are partially supported by grants DOE: DE-FG03-99ER25371, DOD: PET2/ UTA01-347, and the NSF grants: SBR 9873326, ITR EIA-0121523, NPACI 10181410, and Ivan Yotov is partially supported by DOE grant DE-FG03-99ER25371, and the NSF grants: SBR 9873326 and DMS 0107389.

## 7. Appendix

Here we summarize briefly the parameters used in two-phase simulation results presented in the paper. Unless otherwise stated, the two-phase parameters are as follows:

| Symbol              | Meaning   | Value             |
|---------------------|---|-------------------|
| $\mu_o$             | oil viscosity                                       | 2.0000 [cp]       |
| $\mu_w$             | water viscosity                                     | 0.5000 [cp]       |
| $c_o$               | oil compressibility                                 | 0.4000e-04 [/psi] |
| $c_w$               | water compressibility                               | 0.3300e-05 [/psi] |
| $\rho_o$            | oil standard density                                | 56.000 [lb/cu-ft] |
| $\rho_w$            | water standard density                              | 62.340 [lb/cu-ft] |
|                     | porosity  | 0.2               |
|                     | permeability (vertical)                             | 10 [md]           |
|                     | permeability (horizontal)                           | 100 [md]          |
| $S_w^{\text{init}}$ | saturation at reference depth (initial equilibrium) | 0.2               |
| $P_o^{\text{init}}$ | pressure at reference depth (initial equilibrium)   | 500 [psi]         |

Additionally, the parameters used in the multiphysics runs with black-oil model and with single phase model were as follows:

| Symbol   | Meaning                  | Value                           |
|----------|--------------------------|---------------------------------|
| $\mu_o$  | oil viscosity            | 1.0000 [cp]                     |
| $\mu_w$  | water viscosity          | 0.3000 [cp]                     |
| $\mu_g$  | gas viscosity            | 0.015000 [cp]                   |
| $c_o$    | oil compressibility      | varying, approx. 4e-05 [/psi]   |
| $c_w$    | water compressibility    | varying, approx. 1.e-07 [/psi]  |
| $c_g$    | gas compressibility      | varying, approx. 1.4e-03 [/psi] |
| $\rho_o$ | stock tank oil density   | 56.000 [lb/cu-ft]               |
| $\rho_w$ | stock tank water density | 62.343 [lb/cu-ft]               |
| $\rho_g$ | stock tank gas density   | 0.04228 [lb/cu-ft]              |

## References

- [1] L. An, J. Glimm, D. Sharp and Q. Zhang, Scale up of flow in porous media, in: *Mathematical Modeling of Flow through Porous Media*, eds. A.P. Bourgeat, C. Carasso, S. Luckhaus and A. Mikelić (World Scientific, Singapore, 1995) pp. 26–44.
- [2] T. Arbogast, Numerical subgrid upscaling of two-phase flow in porous media, Technical Report 99-30, TICAM, University of Texas at Austin (1999).
- [3] T. Arbogast, L. Cowsar, M.F. Wheeler and I. Yotov, Mixed finite element methods on non-matching multiblock grids, *SIAM J. Numer. Anal.* 37(4) (2000) 1295–1331.
- [4] T. Arbogast, C.N. Dawson, P.T. Keenan, M.F. Wheeler and I. Yotov, Enhanced cell-centered finite differences for elliptic equations on general geometry, *SIAM J. Sci. Comput.* 19 (1998) 404–425.
- [5] T. Arbogast, S. Minkoff and P. Keenan, An operator-based approach to upscaling the pressure equation, in: *Computational Methods in Water Resources XII*, eds. V.N. Burganos et al. (Computational Mechanics Publications, Southampton, 1998) pp. 405–412.
- [6] T. Arbogast, M.F. Wheeler and I. Yotov, Mixed finite elements for elliptic problems with tensor coefficients as cell-centered finite differences, *SIAM J. Numer. Anal.* 34 (1997) 828–852.
- [7] K. Aziz and A. Settari, *Petroleum Reservoir Simulation* (Applied Science, 1979).
- [8] R.P. Batycky, M.J. Blunt and M.R. Thiele, A 3d multi-phase streamline simulator with gravity and changing well conditions, in: *17th Internat. Energy Agency Coll. Project on Enhanced Oil Recovery*, Sydney, Australia, 29 September–2 October 1996.
- [9] F. Ben Belgacem, The mortar finite element method with Lagrange multipliers, *Numer. Math.* 84(2) (1999) 173–197.
- [10] F. Ben Belgacem, The mixed mortar finite element method for the incompressible Stokes problem: Convergence analysis, *SIAM J. Numer. Anal.* 37(4) (2000) 1085–1100.
- [11] L. Bergamaschi, S. Mantica and G. Manzini, A mixed finite element-finite volume formulation of the blackoil model, *SIAM J. Sci. Comput.* 20(3) (1998) 970–997.
- [12] C. Bernardi, Y. Maday and A.T. Patera, A new nonconforming approach to domain decomposition: The mortar element method, in: *Nonlinear Partial Differential Equations and Their Applications*, eds. H. Brezis and J.L. Lions (Longman Scientific & Technical, UK, 1994).
- [13] A. Bourgeat, Homogenized behavior of two-phase flows in naturally fractured reservoirs with uniform fractures distribution, *Comput. Methods Appl. Mech. Engrg.* 47 (1984) 205–216.
- [14] F. Brezzi, L.P. Franca, T.J.R. Hughes and A. Russo,  $b = \int g$ , *Comput. Methods Appl. Mech. Engrg.* 145(3/4) (1997) 329–339.
- [15] M.A. Christie, M. Mansfield, P.R. King, J.W. Barker and I.D. Culverwell, A renormalization-based upscaling technique for WAG floods in heterogeneous reservoirs, in: *Expanded Abstracts* (Society of Petroleum Engineers, 1995) pp. 353–361.
- [16] K.H. Coats, L.K. Thomas and R.G. Pierson, Compositional and black oil reservoir simulator, in: *13th SPE Symposium on Reservoir Simulation*, San Antonio, TX, 12–15 February 1995.
- [17] L.C. Cowsar, J. Mandel and M.F. Wheeler, Balancing domain decomposition for mixed finite elements, *Math. Comp.* 64(211) (1995) 989–1015.
- [18] C.N. Dawson, H. Klie, M.F. Wheeler and C. Woodward, A parallel, implicit, cell-centered method for two-phase flow with a preconditioned Newton–Krylov solver, *Comput. Geosci.* 1 (1997) 215–249.
- [19] J. Douglas, R.E. Ewing and M.F. Wheeler, A time-discretization procedure for a mixed finite element approximation of miscible displacement in porous media, *R.A.I.R.O. Analyse Numerique* 17 (1983) 249–265.
- [20] L.J. Durlofsky, Numerical calculation of equivalent grid block permeability tensors for heterogeneous porous media, *Water Resources Res.* 27(5) (1991) 699–708.
- [21] M.J. Economides and A.D. Hill, *Petroleum Production Systems* (Prentice-Hall, Englewood Cliffs, NJ, 1994).

- [22] H.C. Edwards, A parallel multilevel-preconditioned GMRES solver for multiphase flow models in the implicit parallel accurate reservoir simulator, Technical Report 98-04, TICAM, University of Texas at Austin (1998).
- [23] S.C. Eigenstat and H.F. Walker, Globally convergent inexact Newton method, *SIAM J. Sci. Optim.* 4 (1994) 393–422.
- [24] R. Glowinski and M.F. Wheeler, Domain decomposition and mixed finite element methods for elliptic problems, in: *Domain Decomposition Methods for Partial Differential Equations* (SIAM, Philadelphia, PA, 1988) pp. 144–172.
- [25] T.Y. Hou and X. Wu, A multiscale finite element method for elliptic problems in composite materials and porous media, *J. Comput. Phys* 134(1) (1997) 169–189.
- [26] T.J.R. Hughes, Multiscale phenomena: Green’s functions, the Dirichlet-to-Neumann formulation, subgrid scale models, bubbles and the origins of stabilized methods, *Comput. Methods Appl. Mech. Engrg.* 127(1–4) (1995) 387–401.
- [27] C.T. Kelley, *Iterative Methods for Linear and Nonlinear Equations* (SIAM, Philadelphia, PA, 1995).
- [28] H. Klie, Krylov-secant methods for solving large scale systems of coupled nonlinear parabolic equations, Ph.D. thesis, Rice University, Houston, TX (1996).
- [29] S. Lacroix, Y. Vassilevski and M.F. Wheeler, Iterative solvers of the implicit parallel accurate reservoir simulator (IPARS), to appear in *Numer. Linear Algebra Appl.*
- [30] L.W. Lake, *Enhanced Oil Recovery* (Prentice-Hall, Englewood Cliffs, NJ, 1989).
- [31] Q. Lu, A parallel multi-block multi-physics approach for multi-phase flow in porous media, Ph.D. thesis, The University of Texas at Austin (2000).
- [32] Q. Lu, M. Peszynska and M.F. Wheeler, A parallel multi-block black-oil model in multi-model implementation, in: *2001 SPE Reservoir Simulation Symposium*, Houston, TX, 2001, SPE 66359.
- [33] Q. Lu, M. Peszynska, M.F. Wheeler and I. Yotov, Multiphysics and multinumerics couplings for multiphase flow in porous media, in preparation.
- [34] C.C. Mattax and R.L. Dalton, Reservoir simulation, in: *SPE Monograph Series*, Vol. 13 (Richardson, Texas, 1990).
- [35] N. Moes, J.T. Oden and K. Vemaganti, A two-scale strategy and a posteriori error estimation for modeling heterogeneous structures, in: *On New Advances in Adaptive Computational Methods in Mechanics* (Elsevier, Amsterdam, 1998).
- [36] M. Parashar, J.A. Wheeler, J.C. Browne, G. Pope, K. Wang and P. Wang, A new generation EOS compositional reservoir simulator: Part II – framework and multiprocessing, in: *1997 SPE Reservoir Simulation Symposium*, Houston, TX, 1997, SPE 37977.
- [37] M. Parashar and I. Yotov, An environment for parallel multi-block, multi-resolution reservoir simulations, in: *ISCA 11th Internat. Conf. on Parallel and Distributed Computing System*, September 1998, pp. 230–235.
- [38] D.W. Peaceman, *Fundamentals of Numerical Reservoir Simulation*, 1st ed. (Elsevier Scientific, Amsterdam, 1977).
- [39] D.W. Peaceman, Interpretation of well-block pressure in numerical reservoir simulation with non-square grid blocks and anisotropic permeability, *Trans. AIME* 275 (1983) 10–22.
- [40] G. Pencheva and I. Yotov, Balancing domain decomposition for porous media flow in multiblock domains, in: *Summer Research Conf. on Fluid Flow and Transport in Porous Media: Mathematical and Numerical Treatment* (Amer. Math. Soc., Providence, RI, 2001) to appear.
- [41] M. Peszynska, Advanced techniques and algorithms for reservoir simulation, III: Multiphysics coupling for two phase flow in degenerate conditions, in: *IMA Volumes on Resource Recovery* (submitted August 2000).
- [42] M. Peszynska, E. Jenkins and M.F. Wheeler, Boundary conditions for fully implicit two-phase flow model, submitted.
- [43] M. Peszynska, Q. Lu and M.F. Wheeler, Coupling different numerical algorithms for two phase fluid flow, in: *MAFELAP Proc. of Mathematics of Finite Elements and Applications*, ed. J.R. Whiteman,

- Brunel University, Uxbridge, UK, 1999, pp. 205–214.
- [44] M. Peszynska, Q. Lu and M.F. Wheeler, Multiphysics coupling of codes, in: *Computational Methods in Water Resources*, eds. L.R. Bentley, J.F. Sykes, C.A. Brebbia, W.G. Gray and G.F. Pinder (A.A. Balkema, 2000) pp. 175–182.
- [45] D.K. Ponting, B.A. Foster, P.F. Naccache, M.O. Nicholas, R.K. Pollard, J. Rae, D. Banks and Walsh S.K., An efficient fully implicit simulator, in: *European Offshore Petroleum Conference and Exhibition*, 1980.
- [46] R.A. Raviart and J.M. Thomas, A mixed finite element method for 2nd order elliptic problems, in: *Mathematical Aspects of the Finite Element Method*, Lecture Notes in Mathematics, Vol. 606 (Springer, New York, 1977) pp. 292–315.
- [47] M. Snir, S. Otto, S. Huss-Lederman, D. Walker and J. Dongarra, *MPI: The Complete Reference* (MIT Press, Cambridge, MA, 1996).
- [48] J.A. Trangenstein and J.B. Bell, Mathematical structure of the black-oil model for petroleum reservoir simulation, *SIAM J. Appl. Math.* 49(3) (1989) 749–783.
- [49] P. Wang, I. Yotov, M. Wheeler, T. Arbogast, C. Dawson, M. Parashar and K. Sephernoori, A new generation EOS compositional reservoir simulator: Part I – formulation and discretization, in: *1997 SPE Reservoir Simulation Symposium*, Houston, TX, 1997, SPE 37979.
- [50] M.F. Wheeler, Advanced techniques and algorithms for reservoir simulation, II: The multiblock approach in the integrated parallel accurate reservoir simulator (IPARS), in: *IMA Volume on Resource Recovery* (submitted August 2000).
- [51] M.F. Wheeler, T. Arbogast, S. Bryant, J. Eaton, Q. Lu, M. Peszynska and I. Yotov, A parallel multiblock/multidomain approach for reservoir simulation, in: *1999 SPE Symposium on Reservoir Simulation*, Houston, TX, 1999, SPE 51884.
- [52] M.F. Wheeler, M. Peszynska, X. Gai and O. El-Domeiri, Modeling subsurface flow on pc cluster, in: *High Performance Computing*, ed. A. Tentner (SCS, 2000) pp. 318–323.
- [53] M.F. Wheeler, J.A. Wheeler and M. Peszynska, A distributed computing portal for coupling multiphysics and multiple domains in porous media, in: *Computational Methods in Water Resources*, eds. L.R. Bentley, J.F. Sykes, C.A. Brebbia, W.G. Gray and G.F. Pinder (A.A. Balkema, 2000) pp. 167–174.
- [54] M.F. Wheeler and I. Yotov, Physical and computational domain decompositions for modeling subsurface flows, in: *Tenth Internat. Conf. on Domain Decomposition Methods*, ed. J. Mandel et al., Contemporary Mathematics, Vol. 218 (Amer. Math. Soc., Providence, RI, 1998) pp. 217–228.
- [55] I. Yotov, Mixed finite element methods for flow in porous media, Ph.D. thesis, Rice University, Houston, TX (1996), TR96-09, Department of Comp. Appl. Math., Rice University and TICAM Report 96-23, University of Texas at Austin.
- [56] I. Yotov, A mixed finite element discretization on non-matching multiblock grids for a degenerate parabolic equation arising in porous media flow, *East–West J. Numer. Math.* 5 (1997) 211–230.
- [57] I. Yotov, Interface solvers and preconditioners of domain decomposition type for multiphase flow in multiblock porous media, in: *Advances in Computation: Theory and Practice*, eds. P. Minev, Y. Lin and Y.S. Wong, Vol. 7 (Nova Science, 2001) pp. 157–167.
- [58] T.I. Zohdi, J.T. Oden and G.J. Rodin, Hierarchical modeling of heterogeneous bodies, *Comput. Methods Appl. Mech. Engrg.* 138 (1996) 273–298.